ELECTRICAL CONDUCTIVITY STUDIES ON Y^{3+} AND Mg^{2+}CO-DOPED CERIA ELECTROLYTE SYSTEM

Raúl Alberto Montalvo-Lozano[1], Sagrario Martínez Montemayor[1], Padmasree Karinjilottu Padmadas[2], Antonio Fernandez Fuentes[2]
[1]Facultad de Ciencias Químicas, Universidad Autónoma de Coahuila, V. Carranza esq. J. Cárdenas s/n, Saltillo, Coahuila, México, 25000
[2] Centro de Investigaciones Avanzadas del IPN, Unidad Saltillo, Carretera Monterrey-Saltillo Km. 13, Ramos Arizpe, Coahuila, México, 25900.
contact e-mail: padma512@yahoo.com

ABSTRACT

Doped ceria has been considered as one of the most promising electrolyte materials for intermediate temperature solid oxide fuel cell (IT-SOFC). One of the approaches to further improve the ionic conductivity and other properties is to dope ceria with two or more components. In this work we study the effect of Mg^{2+} doping on the electrical conductivity of yttria doped ceria electrolytes of general formulae $Ce_{0.9}Y_{0.1-x}Mg_xO_{2-\delta}$ (x=0, 0.05) and $Ce_{0.85}Y_{0.15-x}Mg_xO_{2-\delta}$ (x=0, 0.05, 0.1). Powder samples were synthesized by mechanical milling. The phase identification, microstructures and ionic conductivities of the samples were studied by X-ray diffraction, scanning electron microscopy and AC impedance spectroscopy. The results showed that in comparison to singly doped ceria, co-doping with appropriate ratio of Y^{3+} and Mg^{2+} showed higher conductivities and lower activation energies. The bulk, grain boundary and total conductivity of the samples increases with the addition of the dopant and maximum conductivity is obtained for the composition $Ce_{0.9}Y_{0.05}Mg_{0.05}O_{1.925}$. The electrical properties of grain boundary have a large influence due to co-doping than that of the bulk.

Keywords: Oxides, Electrolytes, Conductivity, ceramics.

1. INTRODUCTION

Solid Oxide Fuel Cells (SOFCs) are known to be a promising clean energy technology with many advantages such as high efficiency and material compatibility among the various types of fuel cells [1]. The solid oxide electrolyte is the main component which plays the role of an oxygen ion conductor at high temperature. In oxygen ion conducting solid electrolytes, current flow occurs by the movement of oxygen ions through the crystal lattice as a result of thermally activated hopping of oxygen ions moving from a crystal lattice site to another crystal lattice site. Currently yttria stabilized zirconia (YSZ) is widely used as an electrolyte due to its excellent chemical and mechanical stabilities but it requires high operating temperatures (1000°C) to achieve sufficiently high conductivity. High operating temperature of YSZ electrolyte can lead to complex material problems such as interfacial diffusion between electrodes and electrolyte, mechanical stress due to the different thermal expansion coefficients and durability problems. Therefore, development of solid electrolytes that can be used in the intermediate temperature (e.g., 600-800°C) is important for the future growth of SOFC technology. One of the methods to reduce the operating temperature is to use new electrolyte materials which have higher oxygen ionic conductivity at low temperatures.

The total conductivity of a polycrystalline material consists of both bulk and grain boundary parts and the effect of grain boundary conduction on the performance of an electrolyte are very significant for intermediate and lower temperature applications. The bulk and grain boundary conductivity of the co-doped system varies considerably depending on the chemical nature of the dopants, their concentration and the oxidation state. The grain boundary effect in these polycrystalline samples have been mainly attributed to the presence of highly siliceous amorphous phases, but recent studies have demonstrated that high purity materials also shows this effect and therefore cannot attributed only due to silica contamination [2]. Another possibility is the formation of space charge layer adjacent to the grain boundary is responsible for the low conductivity. It is reported that the addition of alkaline earth oxides increases the grain

boundary conductivity of gadolinium doped ceria to a large extent. The aim of this work is to study the co-doping effect of alkaline earth element like Mg^{2+} to yttria doped ceria system on the ionic conductivity. In order to investigate the co-doping effect of magnesium oxide on yttria doped ceria, two groups of samples with general formula $Ce_{0.9}Y_{0.1-x}Mg_xO_{2-\delta}$ (x=0, 0.05) and $Ce_{0.85}Y_{0.15-x}Mg_xO_{2-\delta}$ (x=0, 0.05, 0.1), were prepared by mechanical milling process.

2. EXPERIMENTAL PROCEDURE

The solid solution with the formula $Ce_{0.9}Y_{0.1-x}Mg_xO_{2-\delta}$ (x=0, 0.05) and $Ce_{0.85}Y_{0.15-x}Mg_xO_{2-\delta}$ (x= 0, 0.05, 0.1), were synthesized by mechanical milling, using high purity (Aldrich, >99+%) CeO_2, Y_2O_3 and MgO as the starting materials. Stoichiometric mixtures of the above chemicals were placed in zirconia containers together with 20 mm diameter zirconia balls as grinding media (balls to powder mass ratio = 10:1). Dry mechanical milling was carried out in air in a planetary ball mill by using a rotating disc speed of 350 rpm. The phase evolution on milling and the sintered sample was analyzed by using X-ray powder diffraction in Philips X'pert Diffractometer using Ni-filtered CuKα radiation (λ=1.5418Å). Specimens for electrical property measurements were pellets obtained by pressing the sample powder in a hydraulic press at a pressure of 5MPa with a diameter of 10 mm diameter and ~ 1 mm thickness. The resulting green pellets were placed in a platinum crucible and sintered at 1500^{o}C for 5 h in air with a slow heating rate of 2°C/minute. The two electrodes were formed by applying platinum paste to either surface of the pellets and then heat treated at 600°C for two hours before the measurement to burn out the binder of the platinum paste and to ensure good contact of the electrodes with the pellet. The transport properties of the sintered pellets were examined by ac impedance spectroscopy over a frequency range 100Hz to 1MHz using Solartron 1260 Frequency Response Analyzer in the temperature range 200-800°C. The impedance data were analyzed using the equivalent circuit of the Z-view software.

3. RESULTS AND DISCUSSION

Figure 1 show the XRD patterns obtained after 1 hr of milling for the single and Mg^{2+} co-

doped samples, and that of pure ceria is also given for reference. The XRD peaks of the samples exhibited all major peaks of a fluorite structure in ceria after 1 h of milling. This may suggest that rare earth and alkaline earth oxides dissolved into ceria. Any additional phase corresponding to the dopants is not observed.

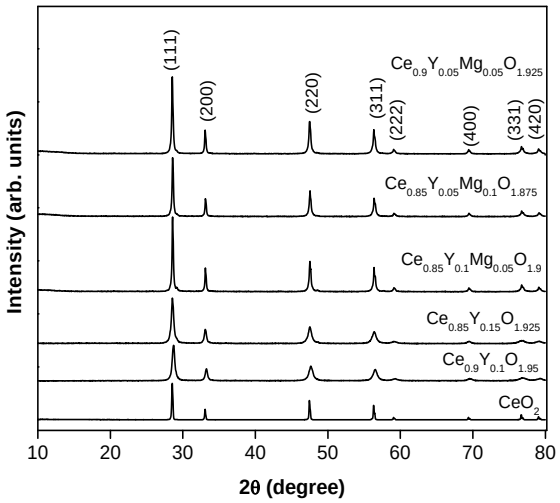

Figure1. XRD patterns obtained after 1 hr of milling for the single and co-doped samples

The ac impedance spectroscopy was applied to determine the electrical properties of singly and co-doped ceria based electrolyte samples. The real ($Z^{'}$) and imaginary ($Z^{''}$) parts of the impedance can be determined by applying a small sinusoidal voltage across the sample and measuring the amplitude and phase angle of the current in a steady state condition. In an impedance plot, the frequency increases from right to the left across the plot. In the ideal case, the ac impedance of an ionic conductor contains the contributions from the bulk, the grain boundaries and electrode-electrolyte interfaces, which can be reflected in a complex plane by three successive semi-circles. The intercept of the high frequency semicircle at the real axis represents the bulk resistance (R_b), the intercept of the intermediate frequency semicircle is the grain boundary resistance (R_{gb}) and the intercept of the low frequency semicircle is the electrode polarization resistance. Therefore, the resistance value at different temperatures can be obtained

and then converted to bulk conductivity (σ_b), grain boundary conductivity (σ_{gb}) and total conductivity (σ_t) using the relation $\sigma=l/AR$, where l and A represent the sample thickness and electrode area of the sample surface, $R = R_b+R_{gb}$ is resistance obtained from the impedance plot respectively.

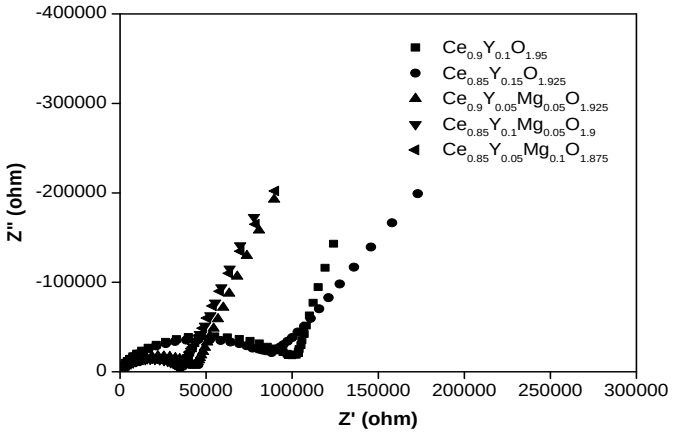

Figure.2. Impedance spectra of $Ce_{0.9}Y_{0.1-x}Mg_xO_{2-\delta}$ (x=0, 0.05) and $Ce_{0.85}Y_{0.15-x}Mg_xO_{2-\delta}$ (x=0, 0.05, 0.1) at 200°C

Fig.2. shows the impedance spectra obtained for $Ce_{0.9}Y_{0.1-x}Mg_xO_{2-\delta}$ (x=0, 0.05) and $Ce_{0.85}Y_{0.15-x}Mg_xO_{2-\delta}$ (x=0, 0.05, 0.1) samples sintered at 1500°C and measured at 200°C in air. In the figure, two features can be observed, an incomplete depressed arc at high frequency and a part of the second arc at low frequency. The high frequency arc is due to the resistive and capacitive effects of the bulk whereas the low frequency arc is related to the blocking of the charge carriers at grain to grain interfaces. From the figure we can see the bulk resistance associated with the co-doped samples is less compared to yttria doped ceria systems. As the measurement temperature is increased, bulk and the grain boundary resistance cannot be separated because with the increase of temperature, the arcs are shifted into high frequencies, which lead to successive disappearance of bulk and grain boundary arc. It is reported that in most cases, the impedance spectra do not exhibit well resolved arcs for bulk and grain boundary contributions due to the limitations of the equipment and to the strong influence of the temperature on the bulk and grain boundary

resistances. Therefore, many authors have assumed that it is possible to extrapolate the grain boundary resistance data and the bulk resistance at high temperature can be determined as the difference between measured total resistance and the extrapolated grain boundary resistance [3].

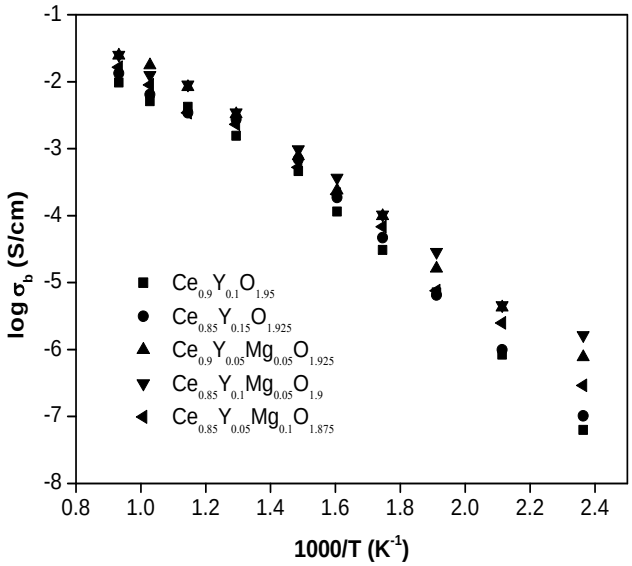

Figure 3. Temperature dependence of the bulk conductivity for single and co-doped samples

The bulk, grain boundary and total conductivity of $Ce_{0.9}Y_{0.1-x}Mg_xO_{2-\delta}$ (x=0, 0.05) and $Ce_{0.85}Y_{0.15-x}Mg_xO_{2-\delta}$ (x=0, 0.05, 0.1) samples sintered at 1500°C are shown in figs. 3, 4 and 5. Since the electrical conduction in these materials are thermally activated, this type of processes is appropriate to be analyzed by the Arrhenius equation:

$$\sigma = \sigma_0 \exp\left(-\frac{E_a}{kT}\right) \qquad (1)$$

where σ_0 is the pre-exponential factor being a constant in certain temperature range, k is the Boltzmann constant, T is the absolute temperature and E_a is the activation energy for ion migration, which is the sum of migration enthalpy (ΔH_m) and the association enthalpy (ΔH_a). The activation energy for the bulk, grain boundary and total conduction is calculated from the slope of the corresponding Arrhenius plot.

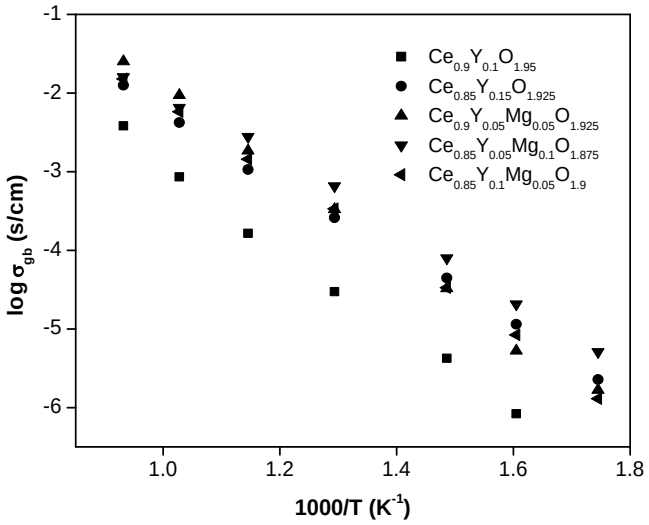

Figure 4. Arrhenius plots for the grain boundary conductivity for the single and co-doped samples

The ionic conductivity increases as the temperature increases, whereas the difference in bulk ionic conductivity decreases with the increase of temperature. The difference in bulk conductivity decreases with the increase of temperature is due to the increase in the concentration of charge carriers arising from the aliovalent doping. . In the low temperature range, the concentration of charge carriers is determined by the thermodynamic equilibrium between the free defects and defect association pairs [4]. The linear behavior of the Arrhenius plot over a wide temperature range indicate the presence of only one type of ion conduction in these electrolyte systems. Co-doped samples showed higher conductivity than singly doped ceria suggesting that co-doping effect exists. The co-doping effect was more obvious in the lower temperature region compared to the higher temperature region.

For the series, $Ce_{0.9}Y_{0.1-x}Mg_xO_{2-\delta}$ (x=0, 0.05), the co-doped system exhibit better electrical properties than the singly doped system and $Ce_{0.9}Y_{0.05}Mg_{0.05}O_{1.925}$ exhibits the highest bulk conductivity (2.58×10^{-2} S/cm) and grain boundary conductivity (3.13×10^{-2}S/cm) at 800°C. Due to the two effect of bulk and grain boundary, the highest total conductivity (1.38×10^{-2}S/cm) is

Table 1. Bulk (σ_b), grain boundary (σ_{gb}) and total (σ_t) conductivity (S/cm) at 800°C and activation energy (E_a) (eV) of $Ce_{0.9}Y_{0.1-x}Mg_xO_{2-\delta}$ (x=0, 0.05) and $Ce_{0.85}Y_{0.15-x}Mg_xO_{2-\delta}$ (x=0, 0.05, 0.1), system sintered at 1500°C for 5 h.

Composition	σ_b	σ_{gb}	σ_t	$E_{a(b)}$	$E_{a(gb)}$	$E_{a(t)}$
$Ce_{0.9}Y_{0.1}O_{1.95}$	1.19×10^{-2}	2.57×10^{-3}	2.02×10^{-3}	0.868	1.061	0.906
$Ce_{0.85}Y_{0.15}O_{1.925}$	1.35×10^{-2}	3.53×10^{-3}	2.80×10^{-3}	0.838	0.893	0.792
$Ce_{0.9}Y_{0.05}Mg_{0.05}O_{1.925}$	2.58×10^{-2}	3.13×10^{-2}	1.38×10^{-2}	0.669	1.001	0.974
$Ce_{0.85}Y_{0.1}Mg_{0.05}O_{1.9}$	2.49×10^{-2}	1.92×10^{-2}	1.08×10^{-2}	0.680	0.962	0.869
$Ce_{0.85}Y_{0.05}Mg_{0.1}O_{1.875}$	1.78×10^{-2}	8.20×10^{-3}	5.39×10^{-3}	0.728	0.985	0.896

given by the composition $Ce_{0.9}Y_{0.05}Mg_{0.05}O_{1.925}$. But in the case of the series, $Ce_{0.85}Y_{0.15-x}Mg_xO_{2-\delta}$ (x=0, 0.05, 0.1), the composition $Ce_{0.85}Y_{0.1}Mg_{0.05}O_{1.875}$ exhibit the highest bulk conductivity (2.49×10^{-2} S/cm) and grain boundary conductivity (1.92×10^{-2} S/cm) at 800°C. For the series $Ce_{0.85}Y_{0.15-x}Mg_xO_{2-\delta}$, the highest total conductivity (1.08×10^{-2}S/cm) is obtained for the composition $Ce_{0.85}Y_{0.1}Mg_{0.05}O_{1.9}$, further increase of MgO leads to a decreases in conductivity. This may be attributed to the very low solubility of Mg^{2+} in the $Ce_{0.85}Y_{0.15}O_{1.925}$ lattice and the segregation Mg^{2+} cations at the grain boundaries with increase in dopant concentration.

Ceria has a cubic fluorite type crystal structure and oxygen vacancies are introduced when it is doped with divalent and trivalent oxides to maintain charge balance, and these oxygen vacancies are responsible for the ionic conduction in these oxides. The formation of oxygen vacancies with the addition of yttrium and magnesium into ceria is represented by the Krö ger-Vink notation as:

$$Y_2O_3 + 2CeO_2 \rightarrow 2Y_{Ce}^{'} + 3O_o^x + V_o^{\bullet\bullet} \qquad (2)$$

$$MgO + CeO_2 \rightarrow Mg_{Ce}^{''} + O_o^x + V_o^{\bullet\bullet} \qquad (3)$$

where $Y_{Ce}^{'}$ or $Mg_{Ce}^{''}$ indicates one Ce^{4+} site occupied by one Y^{3+} or Mg^{2+} ion. Due to coulombic attraction, defect association pairs $(Y_{Ce}^{'}.V_o^{\bullet\bullet}, Mg_{Ce}^{''}.V_o^{\bullet\bullet})$ or $(Y_{Ce}^{'}.V_o^{\bullet\bullet}.Y_{Ce}^{'}, Mg_{Ce}^{''}.V_o^{\bullet\bullet}.Mg_{Ce}^{''})$ are formed between the dopant and the oxygen vacancies. These defect associations or the complexes will prevent the oxygen vacancies from passing through the lattice and result in a decrease of conductivity.

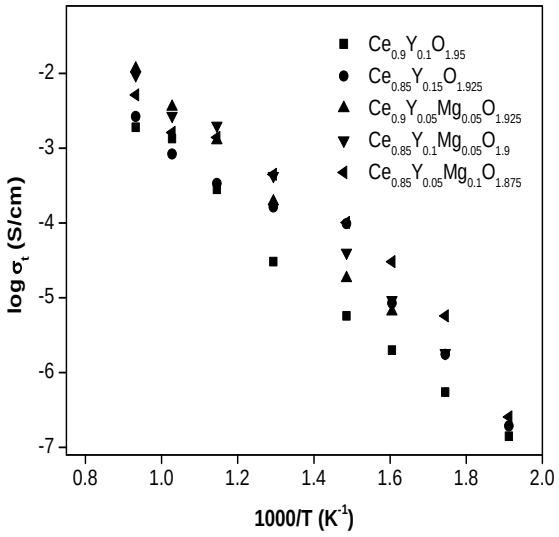

Figure 5. Arrhenius plots for the total conductivity for the single and co-doped samples

It can be noticed from Fig.3 that the Arrhenius plot shows a significant bending which is usually interpreted as a transition from associated to dissociated behavior of the defect cluster or complex. That is in the low temperature region, the activation energy equals to the migration enthalpy and defect association enthalpy and the high temperature region is associated with only the migration enthalpy. A change in slope is observed at around 500-600°C and it indicates the differences in the conduction mechanism at low (150-500°C) and at high (600-800°C) temperatures and the similar results were reported earlier [5]. The change observed at around 600°C can be explained by the changes in the behaviors of the defects in this doped ceria system. In the low temperature range, the oxygen vacancy associated with the dopant is trapped as a result of the association of defects to form defect complexes. Consequently, both the association energy and the migration energy of the system influence the conduction mechanism. At high temperatures, mostly all oxygen vacancies are free and the bulk conductivity is determined by the oxygen ion migration. At the same time, the difference between the bulk conductivities of single and co-doped sample decreases at high temperatures. At low dopant concentration, most of the

oxygen vacancies $V_0^{\bullet\bullet}$ are probably mobile while at high dopant concentrations, defect associations localized near the dopants begin to form at the expense of oxygen vacancies.

Fig.4. shows that the grain boundary conduction increases with the addition of dopants and the maximum grain boundary conductivity is obtained for $Ce_{0.9}Y_{0.05}Mg_{0.05}O_{1.925}$ out of all the studied samples. This may be due to the change in the grain boundary contribution with the increase in dopant concentration and the lowest dopant content result in lowest grain boundary conductivities. The grain boundary activation energy for the low dopant content is greater than the higher dopant content. The decrease in the grain boundary activation energy with increasing the concentration of dopants is perhaps due to the presence of attractive interactions between the dopant cations and oxygen vacancies in the space charge layer leading to an increase in the number of percolation paths. It is confirmed earlier that the accumulation of acceptor cations in the grain boundaries for zirconia and ceria based materials by means of electron energy loss spectroscopy (EELS) and energy dispersive X-ray spectroscopy (EDXS) [6]. Accordingly, a space charge layer model was proposed by Guo and Waser [7], it states a grain boundary consists of a grain boundary core and two adjacent space charge layers at both sides. It has been shown that the grain boundary core of ceria is positively charged and therefore a depletion of oxygen vacancies occurs at the space charge layers. The dopant cations segregate effectively at the grain boundaries as a result of the elastic strain and coulomb interactions, and it leads to the oxygen vacancy depletion in the vicinity of the grain boundaries and affecting the grain boundary properties. Therefore the space charge layers block the oxygen vacancies across the grain boundaries and subsequently the reduction of grain boundary conductivity. When co-doping with a very small amount, the alkaline earth element may perhaps dissolved in the grain boundary suppressing the accumulation of Y^{3+} due to coulomb repulsion, which leads to an increase in oxygen vacancy concentration near the boundary and thus an improvement of grain boundary conductivity. Bin Li et al [8] reported enhanced grain boundary conductivity, when co-doped with MgO and the formation of MgO phases at the grain boundary for higher concentration as evidenced from XRD and FESEM to optimize the space charge regions. Many studies have

shown that as the concentration of the dopant is further increased, the grain boundary conductivity decreases due to the ordering of oxygen vacancies in the space charge layers. For the series, $Ce_{0.85}Y_{0.15-x}Mg_xO_{2-\delta}$ (x=0, 0.05, 0.1), x=0.05 shows the better electrical properties and further increase of the amount of dopant leads to a decrease in both bulk and grain boundary conductivity and in turn a decrease in total conductivity. This may be due to the fact that a very small amount of Mg^{2+} perhaps dissolved in the grain boundary restraining the accumulation of Y^{3+} due to coulomb repulsion, which increases the concentration of oxygen vacancies near the boundary and thus increases the grain boundary conductivity. When the concentration of Mg^{2+} dopant further increases, a majority of Mg^{2+} gathered at the boundary resulting in a highly resistive phase formed at the boundaries thus reducing the grain to grain contacts and thus decreasing the conductivity. We can see from the figure that grain boundary conductivity has the same trend as that of the total conductivity. This is due to the fact that grain boundary makes the primary contribution to the total in polycrystalline electrolytes. Table shows that the change in the grain boundary conductivity is higher than that of the bulk conductivity with the addition of alkaline earth element, which results in an increase in the total conductivity. From the Table, by comparing the activation energy of bulk and grain boundary, we can see that the activation energy of the grain boundary has higher values than that of the bulk, thus confirming that grain boundaries also play a major role on the activation energy of total conductivity. The activation energy of the grain boundary is much higher than that of bulk, So the total activation energy smaller than that of the grain boundary, and grain boundary activation energy is the dominating factor which agree with other results [3,8]. The result suggests that the effect of grain boundary conduction on the performance of electrolyte is very significant for intermediate and lower temperature applications.

Conclusion

The co-doped ceria electrolytes with nominal compositions of $Ce_{0.9}Y_{0.1-x}Mg_xO_{2-\delta}$ (x=0, 0.05) and $Ce_{0.85}Y_{0.15-x}Mg_xO_{2-\delta}$ (x= 0, 0.05, 0.1) were prepared by mechanical milling. The X-ray diffraction patterns of all the synthesized samples confirm the cubic fluorite structure after only 1

hr milling. Co-doping was found to enhance effectively the conductivity of the samples. In comparison to singly doped ceria, co-doping with appropriate ratio of Y^{3+} and Mg^{2+} showed higher conductivities and lower activation energies. The effect of the co-doping on the electrical properties of the grain boundary was more apparent than that of the bulk. The better electrical properties were exhibited by the $Ce_{0.9}Y_{0.05}Mg_{0.05}O_{1.925}$ composition out of all studied samples. It imply that co-doping with optimal ratio of yttria and magnesia can further improve the electrical performance of ceria based electrolytes and these co-doped samples may be better electrolytes for intermediate temperature solid oxide fuel cells.

4. REFERENCES

[1] V.V. Kharton, F.M.B. Marques, A. Atkinson, *Solid State Ionics,* **174,** 135-149 (2004).

[2] T.S.Zhang, J. Ma, S.H. Chan, P. Hing, J.A. Kilner, *Solid State Sciences*, **6,** 565-572 (2004).

[3] D. Pérez-coll, D. Marrero-López, P. Nuñez, J.R. Frade, *Electrochim Acta*, **51,** 6463-6469 (2006).

[4] N Cioatera, V. Parvulescu, A. Rolle, R.N. Vannier, S*olid State Ionics*, **180,** 681-687 (2009).

[5] B Li, Y Liu, Xi Wei, W. Pan, *J. Power Sources*, **195,** 969-976 (2010).

[6] Y Ikuhara, P. Thavoniti, T. Sakuma, *Acta Materialia*, **45,** 5275-5284 (1997).

[7] X Guo, R Waser, *Prog. Mater. Sci*. **51,** 151-210 (2006).

[8] Bin Li, Xi Wei, Wei Pan, *Int. J. Hydro.Energy*, **35,**3016-3022(2010).